American College of Neuropsychopharmacology

ARTICLE

Serotonin modulates an inhibitory input to the central amygdala from the ventral periaqueductal gray

Olivia J. Hon[1], Jeffrey F. DiBerto[1], Christopher M. Mazzone[1], Jonathan Sugam[1], Daniel W. Bloodgood[1], J. Andrew Hardaway[1], Mariya Husain[1], Alexis Kendra[1], Nora M. McCall[1], Alberto J. Lopez[1], Thomas L. Kash[1,2] and Emily G. Lowery-Gionta[1]✉

Fear is an adaptive state that drives defensive behavioral responses to specific and imminent threats. The central nucleus of the amygdala (CeA) is a critical site of adaptations that are required for the acquisition and expression of fear, in part due to alterations in the activity of inputs to the CeA. Here, we characterize a novel GABAergic input to the CeA from the ventral periaqueductal gray (vPAG) using fiber photometry and ex vivo whole-cell slice electrophysiology combined with optogenetics and pharmacology. GABA transmission from this ascending vPAG-CeA input was enhanced by serotonin via activation of serotonin type 2 C ($5HT_{2C}$) receptors. Results suggest that these receptors are presynaptic. Interestingly, we found that GABA release from the vPAG-CeA input is enhanced following fear learning via activation of $5HT_{2C}$ receptors and that this pathway is dynamically engaged in response to aversive stimuli. Additionally, we characterized serotonin release in the CeA during fear learning and recall for the first time using fiber photometry coupled to a serotonin biosensor. Together, these findings describe a mechanism by which serotonin modulates GABA release from ascending vPAG GABA inputs to the CeA and characterize a role for this pathway in fear.

Neuropsychopharmacology (2022) 47:2194–2204; https://doi.org/10.1038/s41386-022-01392-4

INTRODUCTION

In canonical fear models, sensory information from thalamic and cortical areas is conveyed to the lateral and basolateral amygdala [1–4]. Adaptations within these subregions encode associations between fear-inducing stimuli and environmental cues, and form the neurobiological basis for fear learning. Information from the lateral and basolateral amygdala is then conveyed to the central amygdala (CeA), the major output nucleus of the amygdala. The CeA governs fear responses through projections to output structures, namely the periaqueductal gray (PAG) [5].

Disruption of CeA activity impairs fear learning and expression, while stimulation of the PAG elicits defensive responses and disruptions of PAG activity impair conditioned freezing [6–10]. Recently, evidence of plasticity within inhibitory microcircuits in the CeA, as well as inputs from 'upstream' regions like the thalamus following fear learning has broadened the view that adaptations throughout the amygdala underlie fear learning [9, 11–14]. However, mounting evidence indicates that CeA inputs arising from 'downstream' effector targets also influence fear encoding. Recent studies support a role for the PAG in the integration and processing of fear-eliciting stimuli [10, 15–17], and that the PAG modulates other amygdalar subregions [10, 15]. Thus, outputs from the PAG to the amygdala may play a critical role in fear encoding.

The CeA receives inputs from the ventral PAG (vPAG) [18, 19], though the molecular phenotype of this input has not been characterized. The vPAG contains diverse neuronal populations, among the largest of which are GABA neurons [20, 21]. Recent work from our lab shows that chemogenetic inhibition of vPAG GABA neurons during fear learning disrupts fear expression [22]. Others have shown that optogenetic activation and inhibition of vPAG GABA neurons bidirectionally modulate freezing behavior [23], highlighting a key role for this population in fear learning.

Serotonin (5-hydroxy tryptamine, 5HT) has been implicated in the modulation of fear learning [24–26], however, the specific role of 5HT in fear is unknown. We previously showed that 5HT is released in both cortical and amygdalar regions during fear learning [27], while others have shown that 5HT neurons in the dorsal raphe nucleus that project to the CeA are responsive to footshock stimuli [28]. Importantly, 5HT modulates GABAergic transmission in many hubs for affective behaviors [29–31], raising the possibility that 5HT modulation of GABA in the CeA is important for fear encoding.

Here, we demonstrate that vPAG GABA neurons directly project to the CeA to modulate activity and influence fear learning using fiber photometry and ex vivo slice electrophysiology paired with optogenetics and pharmacology. We characterize 5HT release in the CeA and assess 5HT modulation of this pathway and its role in fear-induced plasticity.

METHODS

Animals

All experiments were conducted in accordance with the University of North Carolina at Chapel Hill's Institutional Animal Care and Use Committee's guidelines. Male *Vgat*-ires-Cre mice >8 weeks [32] mice were

[1]Bowles Center for Alcohol Studies, School of Medicine, University of North Carolina at Chapel Hill, Chapel Hill, NC, USA. [2]Department of Pharmacology, School of Medicine, University of North Carolina at Chapel Hill, Chapel Hill, NC, USA. ✉email: emily.g.lowery-gionta.civ@health.mil

Received: 28 March 2022 Revised: 21 June 2022 Accepted: 11 July 2022
Published online: 23 August 2022

used for all input-specific experiments to allow specific targeting of GABA neurons. For all other experiments, male C57BL/6 J mice (Jackson Laboratories, Bar Harbor, ME) were used. All mice were maintained on a 12 h/12 h light/dark cycle with lights on at 7AM. Mice had access to standard rodent chow and water *ad libitum*.

Surgery

Mice were anesthetized using isoflurane (4% induction, 1–2% maintenance). Mice were administered buprenorphine (0.1 mg/kg, s.c.) during surgery, and were also given acetaminophen (80 mg/200 mL in drinking water) one day before and for at least 3 days following surgery. AAV constructs were delivered to the vPAG unilaterally (AP −4.6 mm, ML 0.0, DV- 3.2 mm, 20° angle, 0.5 µl) or CeA bilaterally (AP −1 mm, ML 2.8, DV −4.7, 0.3 µ, 0.1 µl/min) using microsyringes. For photometry experiments, optical fibers were implanted at the same coordinates and cemented to the skull with dental cement (C&B Metabond, Parkell). Mice recovered for >6 weeks prior to the start of experiments.

Fear conditioning

Cued fear conditioning was performed using a three-day protocol. Mice were not habituated to either context prior to conditioning. On day 1 (fear learning), mice were placed into a fear conditioning chamber with a shock grid floor (context A, Med Associates) cleaned with a 20% ethanol+1% vanilla solution. Following a 2 min baseline, 5 tone-shock pairings (tone: 30 s, 80 dB, 3 KHz, shock: 0.6 mA, 2 s) were presented, separated by a random inter-trial interval of 60–90 s. Naïve mice received tones but not shocks. On the second day (context recall), mice were placed into an empty cage for 5 min, then returned to context A for 15 min. On the third day, mice were placed into a novel context with white plastic flooring, curved walls, and cleaned with 0.5% acetic acid. Following a 2 min baseline, 5 tones (identical to fear learning) were presented separated by a random ITI of 60–90 s. Behavior hardware was controlled by Ethovision XT software (Noldus Inc.). Mice for electrophysiology experiments only underwent fear learning, iSeroSnFR mice underwent fear learning and cued recall 24 h later, and GCaMP mice underwent the full 3-day protocol.

Behavior analysis

Behavior was tracked and scored for freezing using open-source, machine learning platforms. First, videos were tracked using DeepLabCut software that uses deep neural networks to estimate mouse position [33]. Tracking information was then analyzed using SimBA, a machine learning platform that can be trained to identify and quantify specific behaviors like freezing [34]. A freezing classifier was developed in-house and then refined such that it did not differ by more than 10% from hand-scoring. Freezing data were processed using a custom MATLAB (Mathworks) script to calculate the % freezing during different epochs, and the start and end time of each freezing bout.

Fiber photometry

For all experiments, optical fibers (200 µm diameter, 0.37 NA, Newdoon Technologies, China) were tested for light transmission prior to implantation. Prior to the start of experiments, mice were habituated daily to patch cord tethering for 3 days. Data were recorded using a Neurophotometrics FP3001 system (Neurophotometrics, San Diego, CA). Briefly, 470 and 415 nm LED light was bandpass filtered, reflected by a dichroic mirror, and focused onto a multi-branch patch cord (Doric, Quebec City, Quebec) by a x20 objective lens. Alternating pulses of 470 and 415 nm light (~50 µW) were delivered at 40 Hz, and photometry signals were time-locked to behavior using a custom built Arduino. Signals were analyzed using custom MATLAB scripts. For all recordings, 470 and 415 signals were deinterleaved and background fluorescence was subtracted. Signals were then lowpass filtered at 5 Hz and fit to a biexponential curve, and the fit was subtracted from each trace to correct for baseline drift. dF/F for both 470 and 415 signals was calculated as (raw signal-fitted signal)/(fitted signal), and traces were then z-scored. Signals were processed further as detailed below.

GCaMP in vPAG^{VGAT} neurons. GCaMP7f (AAV8-syn-FLEX-jGCaMP7f-WPRE, Addgene) was injected unilaterally into the vPAG of *Vgat*-ires-Cre mice and fibers were implanted in vPAG and CeA. After the preprocessing described above, the 415 signal was fit to 470 signal using non-negative robust linear regression to correct for motion [35]. Spike analysis: First, the mean absolute deviation (MAD) of the baseline period (first minute of each recording) was calculated. vPAG spikes were identified using a custom MATLAB script. Peaks with a prominence greater than 2*MAD were included. Alignment with freezing behavior: Freezing behavior was first processed as described above. For vPAG spiking: the timing of each peak was aligned with frame-by-frame freezing data to determine whether each spike occurred during freezing or mobility. For CeA: the start and end time of each freezing bout was extracted. CeA data was segmented based on these timestamps and the average z-score was calculated across all freezing and mobility bouts. Code available at https://github.com/oliviahon/FiberPho.

iSeroSnFR in CeA. iSeroSnFR (AAV9-CAG-iSeroSnFR-nlgn, plasmids provided by Dr. Lin Tian, AAV produced at UNC Vector Core, Chapel Hill, NC) or AAV9-hSyn-EGFP (diluted 1:10 in sterile PBS, Addgene) was injected bilaterally into the CeA of C57Bl/6 J mice to record 5HT release on postsynaptic targets [27]. For iSeroSnFR recordings, 415 signal was not used in analysis as it not an appropriate wavelength for motion control for this sensor. Peri-event plots were generated by normalizing traces to the first 20 s of each trace.

Histology

Mice were transcardially perfused with 30mls each of PBS and 4% paraformaldehyde and brains were post-fixed in 4% PFA for 24 h. Biosensor fluorescence was amplified using immunohistochemistry. Briefly, sections were washed 3 x 5 min in PBS, once in 0.5% Triton-X in PBS, and then 3 x 5 min in PBS. Slices were then incubated in a blocking solution (10% normal donkey serum, 0.1% triton-X in PBS) for 1 h. Slices were incubated overnight in a primary antibody solution (chicken anti-GFP IgY, Aves Labs, Tigard, OR) diluted 1:500 in blocking solution. The following day, sections were washed 3 × 10 min in PBS, and then incubated for 2 h in a secondary antibody solution of donkey anti-chicken IgY conjugated to Alexa-Fluor 488 (Jackson Immunoresearch, West Grove, PA) diluted 1:200 in PBS. Finally, sections were washed 4 × 10 min in PBS. Sections were imaged on a fluorescence microscope, to verify viral expression and fiber placement. Mice with off-target placement were excluded.

Electrophysiology

Whole-cell patch clamp recordings were performed in normal artificial cerebral spinal fluid (ACSF; in mmol/L: 124 NaCl, 4.4 KCl, 2 $CaCl_2$, 1.2 $MgSO_4$, 1 $NaPO_4$, 10 glucose, 26 $NaHCO_3$) on slices prepared from mice sacrificed via deep isoflurane anesthesia as previously described [36, 37].

Vgat-ires-Cre mice were injected with ChR2 in the vPAG and slices containing the vPAG were prepared. Whole-cell patch clamp slice electrophysiology was conducted to characterize action potential firing in response to 1 ms pulses of 490 nM blue light in vPAG^{VGAT} neurons at increasing frequencies (1–100 Hz) using a potassium-gluconate based intracellular solution (in mM: 135 K + gluconate, 5 NaCl, 2 $MgCl_2$, 10 HEPES, 0.6 EGTA, 4 Na2ATP, 0.4 Na2GTP, pH 7.3, 285–290 mOsmol). In the CeA, electrophysiology was conducted to characterize inhibitory post-synaptic currents (IPSCs) evoked by 1–10 ms pulses of 490 nM blue light (Cool LED, Traverse City, MI). Optically-evoked IPSCs (oIPSCs) were isolated by adding the glutamate receptor antagonist kynurenic acid (3 mM; Kyn) to ACSF. Bath application of the GABA-A receptor channel blocker picrotoxin (25 µM) was used to confirm that evoked events were GABAergic. A paired-pulse protocol (2 × 1–10 ms pulses of 490 nM light separated by 50 ms) was used to further investigate the pathway. To evaluate the ratio between the amplitude of the second pulse relative to the amplitude of the first pulse (paired pulse ratio, PPR), the light pulse intensity was adjusted for each cell to reliably elicit 2 time-locked oIPSCs. Following establishment of a stable baseline, 5HT (10 µM, 2 ml/min) was bath applied for 10 min, followed by a 10 min washout. To assess the role of 5HT2C receptors, slices were pre-bathed in ACSF + 5HT2C receptor antagonist RS102221 (5 µM) for at least 20 min. We showed previously that this concentration of 5HT and RS102221 are sufficient to significantly increase GABAergic transmission and to block 5HT2C-mediated depolarization in the extended amygdala, respectively [25].

Whole-cell recordings from the CeA were conducted using kynurenic acid (3 mM) in the bath solution and a potassium-chloride/potassium-gluconate based intracellular solution to isolate GABAergic transmission. 5HT was bath applied as described above. The effects of 5HT on miniature network-independent inhibitory post-synaptic currents (mIPSCs) were assessed using identical parameters as those for sIPSCs with the addition of TTX (1 µM) to the bath solution. Responses to 5HT were defined as a change of greater than 50% of baseline values. Any response that was within 50% of baseline values was classified as no change.

vPAG^{VGAT}-CeA Specific transmission following fear learning. Mice underwent fear learning as described above. 15 min after the session, mice were sacrificed. Using the PPR protocol, basal and 5HT-modulated GABA release from this pathway were evaluated. In addition, the ability of $5HT_{2C}$ receptors to modulate GABA release from this pathway following fear learning was investigated by administering the $5HT_{2C}$ receptor antagonist SB242084 (Tocris, Minneapolis, MN. 3 mg/kg in 10% cremophor + 0.9% saline in a 10 ml/kg i.p.) 30 min prior to the fear learning session (shock group) or 45 min prior to sacrifice (naïve group).

Statistics

Sample sizes for all experiments are based on those commonly used in the literature to assess modulatory effects or between-group differences in slice electrophysiology and behavior experiments. Group numbers are provided in the figure captions. Paired two-tailed *t*-tests were used to assess the effects of 5HT by comparing the final four minutes of 5HT wash on (minutes 11–14) or the final four minutes of washout (minutes 20–23) to the baseline values (minutes 0–4). Between group differences were assessed using unpaired t-tests, two-way ANOVA (treatment x drug) or repeated measures ANOVA with treatment (naïve vs. shock) and time as factors. Where indicated, a priori hypotheses were tested using planned comparison unpaired two-tailed t-tests. Statistical significance was accepted at *p*-values <0.05.

RESULTS

The CeA receives GABAergic inputs from the vPAG

To determine if there is a GABAergic projection from vPAG-CeA, we used whole-cell slice electrophysiology combined with optogenetic stimulation of Cre-inducible ChR2 injected in the vPAG of *Vgat*-ires-Cre mice. We first confirmed that vPAG^{VGAT} neurons expressing ChR2 are activated in response to 1-ms pulses of 490 nM light. We found that vPAG^{VGAT} neurons fire action potentials with 100% fidelity in response to light pulses up to 10 Hz (Fig. 1E–G). To explore the possibility that the CeA receives GABA inputs from the vPAG, we used ChR2-assisted circuit mapping. We discovered terminals in the CeA originating from vPAG^{VGAT} neurons, uncovering a dense nexus of synapses between vPAG^{VGAT} neurons and neurons of the CeA, particularly in the medial CeA (see Fig. 1C, D). Notably, terminals were not visualized in the adjacent BLA which receives inputs from the dorsal PAG [10]. We confirmed our observations by light-evoking oIPSCs in the CeA. oIPSCs were GABA-A receptor mediated, as they were blocked in the presence of picrotoxin but not in the presence of kynurenic acid (Fig. 1H). oIPSCs were detected in 56.86% of cells recorded from the CeA (Fig. 1I). Importantly, this response was time-locked to the light pulse and persisted in the presence of TTX and 4-AP, indicative of a monosynaptic response.

Serotonin is released in the CeA during fear learning

5HT neurons in the DR that project to the CeA are responsive to footshock [28], and we have shown previously that 5HT is released into other subregions of the amygdala during fear learning [27]. Thus, we hypothesized that 5HT is also released in the CeA. To visualize 5HT release, we used fiber photometry coupled to a genetically encoded 5HT sensor, iSeroSnFr. This biosensor is membrane-bound, reliably and selectively detects extracellular 5HT, and can be used to characterize 5HT release in awake and freely-moving rodents when paired with fiber photometry [27]. Using this approach, we recorded 5HT dynamics bilaterally in the CeA (Fig. 2A, B) and found that extracellular 5HT decreases sharply during shock delivery, then rebounds above baseline, peaking roughly 20 s after shock. Both shock and post-shock responses were significantly different from naïve (iSeroSnFR, no shock), and GFP (GFP, shock) controls [shock: $F = 10.94$ $p = 0.0003$ one-way ANOVA, iSeroSnFR fear v. naïve $p = .0014$, iSeroSnFR fear v. GFP $p = 0.0019$, post-shock: $F = 12.32$ $p = 0.0001$, iSeroSnFR fear v. naïve $p = 0.0004$, iSeroSnFR fear v. GFP $p = 0.0023$] (Fig. 2G–K). Notably, 5HT dynamics did not differ between hemispheres (data not shown). Additionally, iSeroSnFR fear mice froze significantly more than naïve mice, indicating that the 5HT sensor did not impair fear learning [$F(122) = 4.846$ $p = 0.0385$ two-way ANOVA] (Fig. 2F). In iSeroSnFR fear mice, the post-shock response significantly decreased between the first and last presentations [$t(12) = 2.431$ $p = 0.0317$ paired *t*-test] (Fig. 2L, M). No changes were detected in iSeroSnFR naïve or GFP shock mice, indicating that this change is likely physiological and not due to photobleaching. One day following fear learning, fear expression was tested in a cued recall test and 5HT dynamics were recorded. Responses to tone presentations did not differ statistically between groups (Fig. S1C–F), though freezing was significantly higher in fear mice [Fig. S1G, $F(1\ 23) = 30.18$, $p < 0.0001$ two-way ANOVA).

The vPAG^{VGAT}-CeA input is modulated by 5HT directly and via presynaptic $5HT_{2C}$ receptors

5HT has been shown previously to modulate GABAergic transmission in the CeA [38], thus we postulated that 5HT may also control GABA release from vPAG^{VGAT} terminals. To test this hypothesis, we expressed Cre-inducible ChR2 in the vPAG of *Vgat*-ires-Cre mice and recorded oIPSCs evoked by a 1 × 1–10 ms pulse of light or oIPSCs evoked by 2 × 1–10 ms pulses of light separated by a 50 ms interpulse interval in the CeA. In all cells tested, 5HT significantly enhanced the amplitude of the first oIPSC [$t(12) = 4.562$, $p = 0.0007$ for baseline v. 5HT; Fig. 3B–D], an effect that did not wash out [$t(12) = 3.539$, $p = 0.0041$ for baseline v. washout; data not shown], demonstrating that 5HT enhances GABA transmission at vPAG synapses with CeA neurons. In addition, 5HT significantly reduced the paired-pulse ratio (PPR) [$t(5) = 2.817$, $p = 0.0372$ for baseline v. 5HT; $t(5) = 4.202$, $p = 0.0085$ for baseline v. washout; Fig. 3E], suggesting 5HT enhances GABA release at vPAG synapses on to CeA neurons presynaptically. To determine if this effect is direct, we isolated direct transmission by adding TTX and 4-AP to the bathing solution. We found that the ability of 5HT to enhance GABA release persisted in the presence of TTX and 4-AP [$t(3) = 10.98$, $p = 0.0016$ amplitude of first peak baseline v. 5HT; $t(3) = 6.577$, $p = 0.0072$ PPR baseline v. 5HT], strongly suggesting that 5HT acts directly at the vPAG^{VGAT}-CeA synapses to enhance GABA release (Fig. 3F–I). The $5HT_{2C}$ receptor is Gq-coupled and modulates GABA release in the amygdala [31, 38, 39], and so we surmised that it may mediate 5HT effects on GABA release from vPAG terminals. We found that the ability of 5HT to enhance GABA release from the vPAG^{VGAT}-CeA input was blocked in the presence of the $5HT_{2C}$ antagonist RS102221 [$t(4) = 1.122$, $p = 0.3248$ amplitude of the first peak baseline v. 5HT; $t(4) = 1.477$, $p = 0.2137$ PPR baseline v. 5HT; see Fig. 3J–M], supporting the idea that presynaptic $5HT_{2C}$ receptors potentiate GABA release in this pathway.

To explore whether these effects were consistent across the general medial CeA, we recorded spontaneous IPSCs in the CeA of C57BL/6 J mice. 5HT (10 µM) enhanced the frequency [$p < 0.0465$ $t(10) = 2.271$] (Fig. S2B, C), but not amplitude (Fig. S2A, C) of sIPSCs in 63.6% of recorded cells (Fig. S2D) suggesting that overall 5HT enhances presynaptic GABA release in the medial CeA. 5HT enhanced the frequency but not amplitude of mini IPSCs (mIPSCs) recorded in the presence of TTX (1 µM) only in a subset of cells (Fig. S2E–H), suggesting that the majority of this effect appears to be polysynaptic. $5HT_{2C}$ antagonist RS102221 partially blocked 5HT enhancement of sIPSC frequency in the medial CeA (Fig. 2J–L), without altering amplitude (Fig. S2I, K), though overall this effect was not statistically significant. Of cells recorded, 54.5% showed an increase in GABA release in response to 5HT, 36.4% showed a decrease and 9.1% showed no change (Fig. S2L).

Fear learning induces plasticity at vPAG^{VGAT}-CeA inputs

We previously showed that chemogenetic inhibition of vPAG^{VGAT} neurons during fear learning impairs later fear expression [22]. Taken with our findings that 5HT is released in the CeA during fear learning and modulates GABA release from vPAG^{VGAT}-CeA inputs via $5HT_{2C}$ receptors, we hypothesized that fear learning may alter 5HT-induced

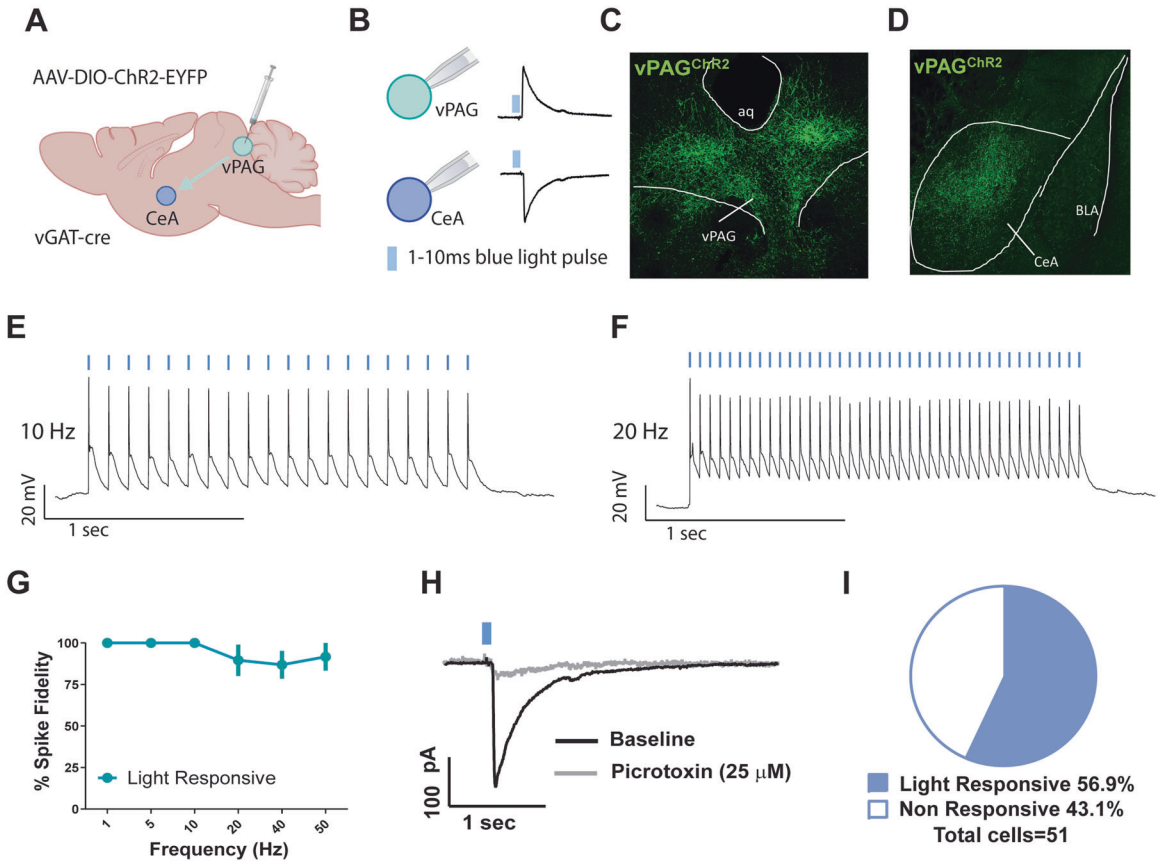

Fig. 1 vPAG GABA neurons have functional projections to the CeA. A surgical schematic of channelrhodopsin infusion into the vPAG of *Vgat*-ires-Cre mice. **B** schematic of responses in vPAG and CeA upon blue light stimulation. **C**, **D** Representative image showing expression of channelrhodopsin (ChR2) in the vPAG of a *Vgat*-ires-Cre mouse. **E**, **F** Representative action potential firing at 10 Hz and 20 Hz. **G** Fidelity of action potential spiking in response to ChR2 activation by 1 ms pulses of blue 490 nM light in vPAG GABA neurons (c; $n = 6$ cells from 5 mice). **H** representative average trace of inhibitory post-synaptic potentials evoked by 1 ms pulses of blue 490 nM light (oIPSCs) recorded from a cell of the CeA proximal to ChR2 terminal expression in the absence and presence of the GABA-A ion channel blocker picrotoxin (25 μM). **I** Percent of cells recorded from in the CeA proximal to ChR2 terminal expression that showed oIPSCs in response to blue 490 nM light stimulation ($n = 51$ cells).

GABA release from vPAG^{VGAT}-CeA inputs via this mechanism. To test this hypothesis, we put intra-vPAG ChR2-expressing *Vgat*-ires-Cre mice through fear learning. 15 min after the session, we prepared slices containing the CeA for electrophysiology (Fig. 4A, B) and recorded the effects of 5HT (10 μM) on optically evoked oIPSCs from mice that underwent fear learning (fear) or control mice (naïve). Results showed that the ability of 5HT to enhance GABA release was blunted in fear mice relative to naïve mice (Fig. 4C), evidenced by a significant change in the amplitude of the first evoked peak [$F(14,168) = 3.258$, $p = 0.0001$ time x treatment interaction; $F(14, 168) = 19.57$, $p < 0.0001$ main effect of time; $F(112) = 10.30$, $p = 0.0075$ main effect of treatment, two-way RM ANOVA]. Post-hoc analyses revealed between-group differences at minutes 8, 10, and 13–14 [$p < 0.05$ for all Bonferroni multiple comparisons tests]. (Fig. 4C). Significant between-group differences in the effects of 5HT on the amplitude of the first oIPSC were observed [see Fig. 4D; $F(112) = 8.805$, $p = 0.0118$ fear x 5HT interaction; $F(112) = 30.94$, $p = 0.0001$ for main effect of 5HT; $F(112) = 8.157$, $p = 0.0145$ main effect of fear, two-way RM ANOVA]. Post-hoc analyses show that 5HT significantly enhanced the amplitude of the first oIPSC relative to baseline values in naïve but not fear mice [$p < 0.0001$ Bonferroni post-hoc test for multiple comparisons], indicating that the ability of 5HT to enhance the amplitude of the first oIPSC was significantly blunted in fear mice. Taken together, these data may reflect an engagement of the vPAG^{VGAT}-CeA pathway during fear learning, occluding further effects of 5HT.

To examine this possibility, we compared PPR from fear or naïve mice that were pretreated with $5HT_{2C}$ antagonist SB242084 or vehicle (Fig. 4E). We hypothesized that in vivo pretreatment with SB242084 would block engagement of $5HT_{2C}$ receptor signaling at the vPAG^{VGAT}-CeA input during fear learning. Among mice that were not pretreated with SB24284, we found that fear mice had significantly lower PPRs than naïve mice [$p = 0.0452$, $t(21) = 2.129$ unpaired *t*-test] (Fig. 4F). Notably this effect of fear was blocked by pretreatment with SB24284, as fear mice pretreated with the drug had significantly higher PPRs than fear mice that received vehicle [$p = 0.0476$, $t(21) = 2.104$ unpaired *t*-test]. Pretreatment with SB242084 did not alter PPR in naïve mice relative to vehicle [$p = 0.8286$, $t(15) = 0.2203$ unpaired *t*-test]. These a priori hypotheses reflect between group differences, however a two-way ANOVA performed on this data set was not significant [$F(137) = 1.727$, $p = 0.1968$ for the condition x drug interaction; $F(137) = 1.933$, $p = 0.1727$ main effect of drug; $F(137) = 0.3345$ main effect of condition].

vPAG^{VGAT}-CeA is dynamically engaged during fear and responds to footshock

To characterize vPAG^{VGAT}-CeA activity in vivo, we used fiber photometry coupled to the genetically encoded calcium indicator GCaMP7f to simultaneously record vPAG^{VGAT} cell bodies and terminals in the CeA during fear learning (Fig. 5A±C). We found that overall, cell body (vPAG) and terminal (CeA)

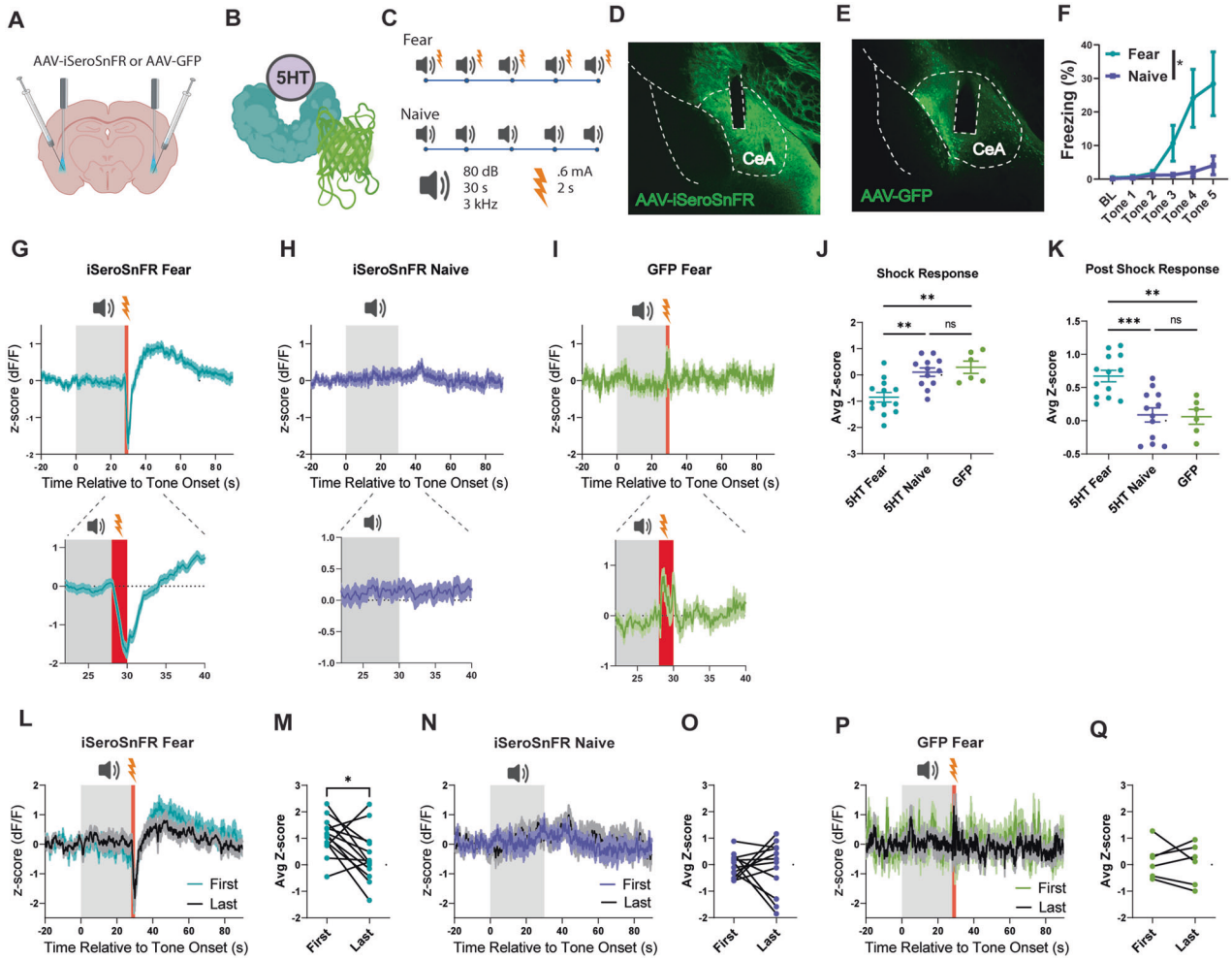

Fig. 2 5HT is released in the CeA during fear conditioning. A schematic of injections and fiber implant for iSeroSnFR recordings. **B** schematic of iSeroSnFR. **C** Schematic of tones and shocks presented during fear learning for fear and naïve groups. **D, E** Representative image of iSeroSnFR and GFP and optic fiber placement in CeA. **F** Freezing behavior during fear learning. Response to tone and shock presentations averaged across cohort for iSeroSnFR Fear (**G**), iSeroSnFR Naïve (**H**), and GFP Fear (**I**). Zoomed in traces show shock responses. **J** shock response averaged from $t = 28–30$ relative to tone onset across all trials. **K** post-shock response averaged from $t = 33–60$ relative to tone onset across all trials. Responses to first and last tone/shock presentations averaged across cohort for iSeroSnFR Fear (**L**), iSeroSnFR Naive (**N**), and GFP fear (**P**). Average post-shock response for first and last trials for iSeroSnFR Fear (**M**), iSeroSnFR Naive (**O**), and GFP fear (**Q**). $n = 13$ iSeroSnFR fear, 11 iSeroSnFR naïve, 6 GFP fear.

activity was highly similar (Fig. 5D, H). In fear mice, both vPAG and CeA responded to tone onset and shock, indicated by significant increases in average z-score compared to baseline [$t(7) = 3.843$ $p = .0063$ CeA tone response v BL, $t(10) = 4.473$ $p = 0.0012$ vPAG tone response v BL, $t(7) = 5.284$, $p = 0.0011$CeA shock response v. BL, $t(10) = 11.31$, $p < 0.0001$ for vPAG shock response v. BL, paired t-test] (Fig. 5D–G). Naïve mice did not show significant engagement of either region in response to tone onset (Fig. 5H–J), suggesting that vPAG^{VGAT}-CeA encodes responses to fear-evoking stimuli.

We next asked whether differences in fear and naïve mice could be detected during fear expression. One day after fear learning, we returned mice to the fear chamber for 15 min to characterize activity during context recall. Baseline activity was recorded for 5 min in a neutral, familiar environment prior to returning the mice to the fear chamber in order to capture any shifts in activity. We did not find significant differences between groups in either vPAG or CeA activity (Fig. S3C–E). One day after context recall, mice underwent a cued recall test. Responses to tone presentations were quantified, and no differences were found in vPAG or CeA activity between groups (Fig. S3J–L).

vPAG^{VGAT} neuron activity negatively correlates with freezing behavior

We previously showed that vPAG^{VGAT} neurons drive fear conditioning [22], and others have reported that vPAG^{VGAT} cells bidirectionally modulate freezing behavior [23]. However, it is unknown if information about freezing is communicated via projections to the CeA. Therefore, we explored the relationship between vPAG^{VGAT}-CeA activity and freezing by using machine learning-based algorithms to extract frame-by-frame behavior information (Fig. 5K). Comparison of photometry and behavior data revealed an inverse relationship between freezing and both vPAG^{VGAT} cell body and terminal activity. During fear learning, fear mice froze significantly more than naïve mice, and had significantly lower vPAG spike frequency [freezing: two-way RM ANOVA $F(1,16)=56.82$ $p < 0.0001$ main effect of fear, Spike frequency: $F(116)=5.505$ $p = 0.0322$ main effect of fear] (Fig. 5L, O). We next aligned freezing and vPAG spiking data to classify spikes as either occurring during freezing or mobility. We found that overall, vPAG spike frequency was significantly lower during freezing than mobility, indicating that vPAG activity is suppressed during freezing [two-way ANOVA $F(116) = 52.49$,

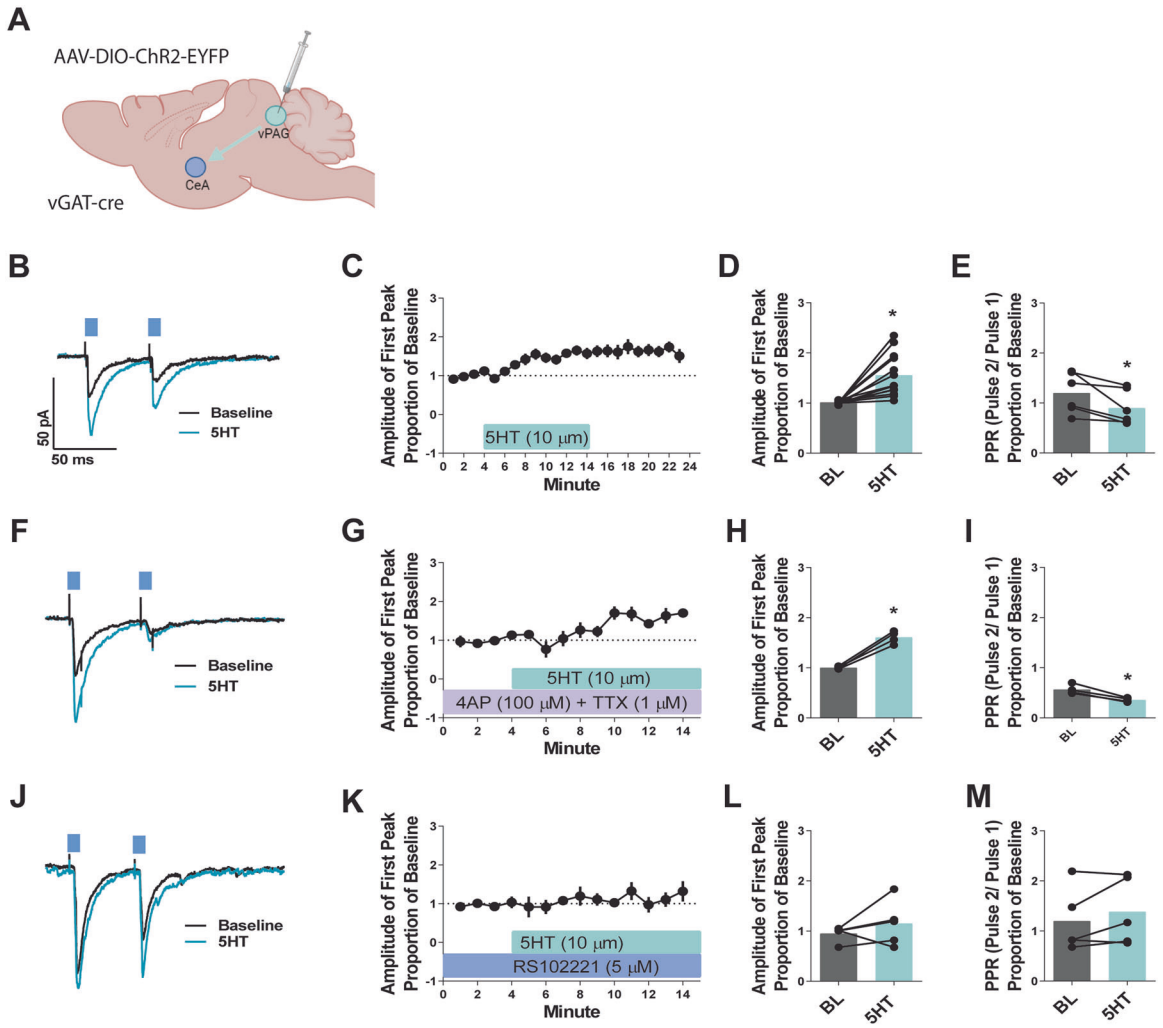

Fig. 3 The vPAG^{Vgat}-CeA pathway is modulated by serotonin directly and via presynaptic 5HT2C receptors. A surgical schematic of channelrhodopsin infusion into the vPAG of *Vgat*-ires-Cre mice. **B** Representative traces showing oIPSCs at baseline and during serotonin bath application. **C, D** Time course and summary of the effects of bath application of serotonin (10 μM) on the amplitude of the first evoked peak relative to baseline values ($n = 13$ cells from 9 mice). **E** Summary of the effects of serotonin on the paired pulse ratio (PPR; amplitude of pulse 2/ amplitude of pulse 1) ($n = 6$ cells from 4 mice).Time course and summary of the effects of serotonin on the amplitude of the first evoked peak (**F**, **G**) and PPR (**H**, **I**) in the presence of 4-Aminopyridine (4 AP; 100 μM) and tetrodotoxin (TTX; 1 μM) ($n = 4$ cells from 2 mice). **J**–**M** Time course and summary of the effects of serotonin on the amplitude of the first evoked peak and PPR in the presence of the 5HT2C antagonist RS102221 (5 μM) ($n = 5$ cells from 4 mice). $^{*}p < 0.05$; all data shown as means +/− SEM.

$p = 0.0001$ main effect of freezing, $F(116) = 0.1275$ $p = .7257$ group x freezing interaction] (Fig. 5N). To determine whether vPAG^{VGAT} terminal activity is also suppressed during freezing, we extracted the start and end times of each freezing bout and parsed CeA data points as occurring during either freezing or mobility. We then took the average of each group. We chose to look at average activity in terminals because this method of calcium imaging is not sensitive enough to record spikes in terminals. Consistent with what we observed in cell bodies, activity in terminals is lower during freezing compared to mobility [two-way ANOVA $F(113) = 7.959$, $p = 0.0144$ main effect of freezing] (Fig. 5Q). Notably, this effect was independent of whether mice underwent fear conditioning.

During context recall, fear mice exhibited higher freezing than naïve mice, but we did not find a difference in spike frequency across groups [freezing: $F(116) = p = 0.0002$ main effect of fear] (Fig. S3). However, spike frequency in vPAG and average signal in CeA were significantly lower during freezing bouts, consistent with fear learning [vPAG: two-way ANOVA $F(116) = 69.84$ $p = 0.0001$ main effect of freezing, CeA: two-way ANOVA $F(112) = 15.41$ $p = 0.002$ main effect of freezing] (Fig. S3H, I). Similar effects were also present during cued recall. Fear mice froze more than naïve mice, had lower vPAG spike frequency, and lower activity during freezing compared to mobility [freezing: two way RM ANOVA $F(116) = 6.837$ $p = 0.0188$ for main effect of fear, vPAG spike frequency: two way RM ANOVA $F(116) = 5.457$ $p = 0.0328$ main effect of fear, vPAG spiking during freezing: $F(115) = 24.65$ $p = 0.0002$ main effect of freezing, CeA: $F(113) = 23.38$ $p = 0.0003$ main effect of freezing] (Fig. S3M–P).

DISCUSSION

The current experiments identify a GABAergic input to the CeA from the vPAG that is modulated by serotonin via presynaptic $5HT_{2C}$ receptors. We find that plasticity occurs in this pathway following fear learning and is mediated by $5HT_{2C}$. Together, these data demonstrate that the vPAG has inhibitory influence over the CeA and adds to a growing body of evidence that PAG projections to 'upstream' structures inform conditioned fear processes.

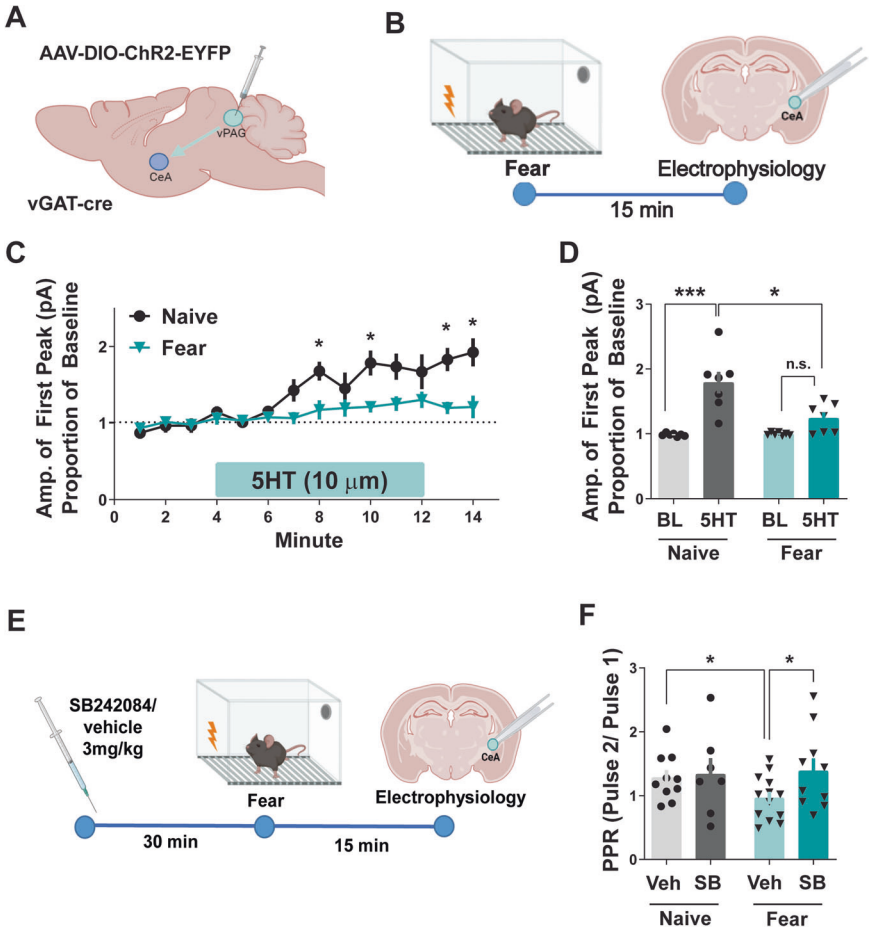

Fig. 4 Fear learning engages the vPAG^{Vgat}-CeA pathway. A surgical schematic of channelrhodopsin infusion into the vPAG of *Vgat*-ires-Cre mice. **B** Experimental timeline for fear conditioning and electrophysiology experiments. **C**, **D** Time course and summary of the effect of bath application of serotonin (5HT; 10 μM) on the amplitude of the first evoked peak relative to baseline values in shock mice versus naïve mice ($n = 7$ cells per group from 3 mice per group), recordings in CeA. **E** Experimental timeline for fear conditioning and electrophysiology experiments with $5HT_{2c}$ antagonist pretreatment. Mice were administered the 5HT2C antagonist SB242084 (3 mg/kg, i.p.) or vehicle prior to the fear acquisition session (shock) or 45 min prior to sacrifice (naïve) and recordings were performed at terminals in the CeA. **F** Summary of the effects of serotonin on the paired pulse ratio (PPR; amplitude of pulse 2/amplitude of pulse 1) in shock or naive mice that did or did not receive drug (e; $n = 7$–13 cells per group from 3–5 mice per group). $^{*}p < 0.05$; all data shown as means +/− SEM.

Non-canonical ascending outputs from the vPAG-CeA

While descending amygdalar inputs to the PAG and their role in fear behavior have been well-established, reciprocal ascending inputs from the PAG to the amygdala are of growing interest [10, 40]. Retrograde tracing studies have shown that cells of the vPAG innervate the CeA [18, 19] but the cellular phenotype of these cells had not been characterized. The current results extend these findings by identifying GABA neurons as one population of vPAG neurons that robustly innervate the CeA. These findings demonstrate that the vPAG has inhibitory influence over the CeA and is anatomically and functionally poised to regulate CeA microcircuits and perhaps overall amygdalar output.

Serotonin dynamics in the CeA

5HT neurons in the DRN that project to the amygdala are engaged during fear learning and extinction [28, 41], but the dynamics of 5HT release in the CeA has not been characterized. Microdialysis studies have shown that 5HT levels in the BLA are elevated after fear recall [8] and in both the BLA and CeA in response to noxious stimuli [42, 43], but this technique can only measure 5HT levels on the scale of minutes. Additionally, DRN^{5HT} neurons co-express a variety of neurotransmitters [28, 41, 44], thus activity of DRN^{5HT} neurons does not necessarily reflect downstream release of 5HT. Recent advances in biosensor imaging allow for visualization of 5HT release with millisecond temporal resolution and high specificity, providing a level of detail not attainable with other methods. We show for the first time that 5HT release in the CeA is dynamic during fear learning, consisting of both increases and decreases in extracellular levels. Additionally, we show that 5HT is released specifically in response to shock but not tone, and changes over the course of fear learning. Previous studies show that CeA-projecting DRN^{5HT} cells are activated by shock [28], consistent with the upward response we observe after shock end. However, the downward spike during shock has not been documented before and may be driven by modulation of DR 5HT terminals. Importantly, we did not see a similar response in GFP controls, indicating that both the upward and downward components of the shock response are driven by 5HT and not motion.

Serotonin modulation of GABAergic signaling in CEA

Our results show that serotonin robustly and reliably enhances GABA-mediated synaptic transmission from the vPAG-CeA input, and drives increased frequency of GABAergic events. These observations support the position that 5HT enhances presynaptic GABA transmission without effects on post-synaptic transmission. $5HT_{2C}$Rs are expressed in the vPAG and the CeA, so it remains possible that there are multiple mechanisms at play. Additionally, we showed that the effect of 5HT was long-lasting and did not

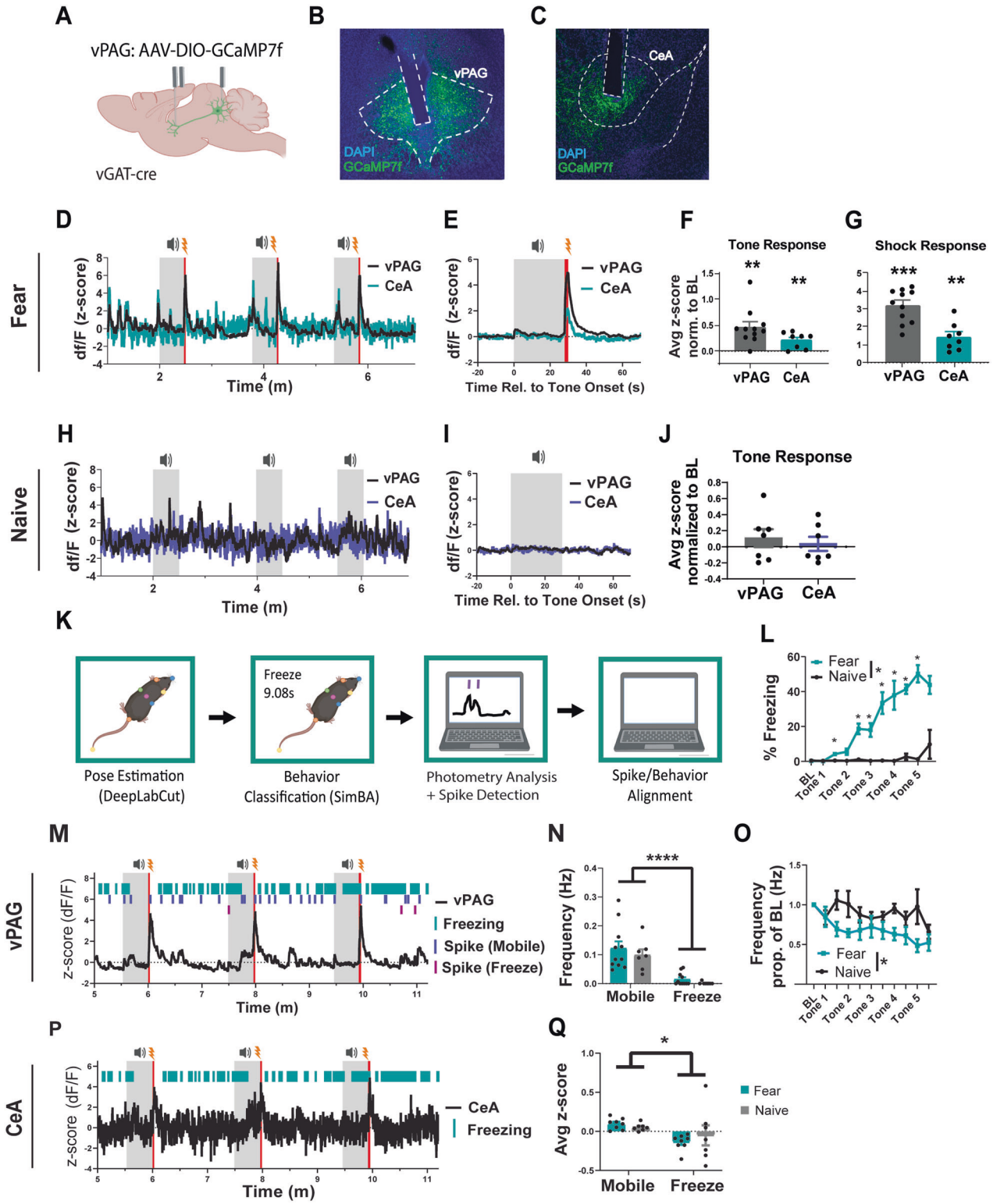

wash out, which may indicate a form of plasticity. This effect persisted in the presence of TTX, demonstrating that modulation of GABA release at this input is direct and does not require an intervening network. We also found evidence that serotonin enhances GABA release in the general medial CeA population, but unlike the input-specific effect, 5HT-mediated enhancement of GABA release was reduced in the presence of TTX. As such, serotonin's modulation of GABA release within the CeA appears to be more varied in the general population. Together, these results reveal a novel and complex role for serotonin in modulating inhibitory transmission within the CeA. We do note that one important limitation of this study is that the number of recordings for the TTX + 4AP experiment is only four, however the effect is robust and consistent.

Based on observations that the $5HT_{2C}$ receptor modulates GABA release in the CeA [38], we hypothesized that serotonin's

Fig. 5 vPAG^{Vgat}-CeA pathway is dynamically engaged during fear learning and responds to shock-predicting cues. A surgical schematic of GCaMP7f infusion into the vPAG of *Vgat*-ires-Cre mice. **B**, **C** representative image of GCaMP expression and fiber placement in vPAG and CeA . **D** Representative trace showing vPAG and CeA signal during fear learning in a mouse that underwent fear conditioning. **E** vPAG and CeA responses to tone/shock presentation in fear conditioned mice averaged across cohort. **F** Tone response calculated as the average from $t = 0$–5, normalized to $t = -5$–0 relative to tone onset. **G** Shock response calculated as the average from $t = 28$–30, normalized to $t = 23$–28 relative to tone onset. **H** Representative trace showing vPAG and CeA signal during learning in a naïve mouse. **I** vPAG and CeA responses to tone presentation in naïve mice averaged across cohort. **J** Tone response calculated as the average from $t = 0$–5, normalized to $t = -5$–0 relative to tone onset. **K** schematic of analysis pipeline for alignment of freezing and photometry signal. **L** Freezing behavior during fear learning. **M** Representative trace showing alignment of freezing and vPAG signal with identified spikes classified as occurring during freezing (magenta) or mobility (purple). **N** vPAG spike frequency during freezing and mobility for fear mice (turquoise) and naïve (gray). **O** vPAG spike frequency during each epoch of fear learning, normalized to BL. **P** Representative trace showing alignment of freezing and CeA signal. **Q** average signal during freezing and mobility averaged across all bouts. $n = 10$ vPAG fear, 7 vPAG naïve, 8 CeA fear, 7 CeA naïve.

effects in the CeA may involve the $5HT_{2C}$ receptor. In agreement with this hypothesis, we found that 5HT enhancement of GABA release from the vPAG-CeA input was abolished by a $5HT_{2C}$ antagonist. Because $5HT_{2C}$R blockade prevented this effect, measured via PPR, we conclude that these receptors have a pre-synaptic locus of action. Generally, $5HT_{2C}$ receptors are thought to be located at post-synaptic sites, where they control cellular excitability [39]. However, a pre-synaptic locus of action has been previously shown, evidenced by findings that receptors co-localize with pre-synaptic proteins [45] and modulate GABA release in the VTA in a calcium-dependent manner [31]. Thus, pre-synaptic $5HT_{2C}$ receptors that control neurotransmitter release do not appear to be unique to the CeA. In contrast, we found that 5HT enhancement of GABA transmission in the general CeA is only partially blocked by $5HT_{2C}$ receptors, suggesting that additional 5HT receptors modulate GABA release in the greater CeA. Therefore, serotonin may finely tune inhibitory transmission within the CeA in a synapse-specific manner, with $5HT_{2C}$ receptors restricted to select synaptic nodes like those arising from vPAG^{VGAT} inputs. We do note that one important limitation of this study is that for these plasticity experiments, the sample size ranges from 7–13 cells.

A locus for 5HT modulation of fear response in the CeA

Within the CeA, adaptations in excitatory transmission are observed following fear learning that are likely driven by glutamatergic inputs from the BLA, lateral amygdala, paraventricular nucleus of the thalamus, or cortex [12–14, 46]. Enhancements in inhibitory modulation have also been reported, though from unidentified sources [47]. The current findings suggest that plasticity at the vPAG-CeA input may support fear learning by encoding sensory responses to footshock and cues. Specifically, we observed that GABA release from this input was augmented following fear learning. Additionally, 5HT's ability to further facilitate GABA release from this input was disrupted following fear learning, suggesting plasticity had occurred at the vPAG-CeA input. This finding is consistent with the hypothesis that the 5HT-GABA system is engaged endogenously during fear learning, thereby occluding the ability of 5HT to elicit further GABA release in slice recordings. We confirmed this possibility by blocking $5HT_{2C}$ receptors in vivo prior to fear learning, which resulted in normalized GABA release from the vPAG-CeA input. Based on these findings and the model revealed through characterization of the vPAG-CeA input, we posit that serotonin activates presynaptic $5HT_{2C}$ receptors in the medial CeA in response to footshock, which stimulates GABA release from the vPAG-CeA input (Fig. S4). As such, it appears that serotonin recruits the vPAG's inhibitory modulation of the medial CeA.

Dynamic engagement of the vPAG^{VGAT}-CeA pathway in response to fear-evoking stimuli

It has been previously shown that vPAG GABA neurons bidirectionally modulate freezing behavior, and optogenetic inhibition and activation of GABA neurons increase and decrease freezing behavior respectively [23]. Consistent with this, we found that activity in vPAG^{VGAT} cell bodies and terminals in CeA is lower during freezing than mobility. However, this effect was independent of whether mice underwent fear learning and thus suggests that vPAG^{VGAT} neurons modulate freezing behavior under basal conditions, a property that is not altered by fear learning. Notably, our findings suggest an additional role for vPAG^{VGAT} cells in fear beyond modulation of freezing. We previously reported that chemogenetic inhibition of vPAG^{VGAT} cells during fear learning impaired subsequent fear expression [22], and in the current study, we show that fear learning induces plasticity in vPAG projections to CeA. Taken together, this suggests fear-specific alterations in signaling in this pathway. To test this hypothesis, we used fiber photometry to record VGAT cell bodies in vPAG and terminals in CeA during fear. We found that vPAG^{VGAT} cell bodies and terminals were responsive to both tone and shock in fear mice. Importantly, vPAG^{VGAT}-CeA was not responsive to tone in naïve mice, suggesting that vPAGVGAT cells specifically relay aversive sensory information during fear. Taken together with recent findings that ventrolateral PAG neurons encode the size of a threat [48, 49], our data implicate the vPAG in more complex fear encoding processes than previously thought. Additionally, we did not see differences in vPAG^{VGAT}-CeA activity between fear and naïve mice during context or cued recall, indicating that this pathway is important for the acquisition but not expression of conditioned fear.

Using automated tracking to identify relationships between behavior and cellular activity

Recent advances in open-source rodent behavior tracking technology allows for fast, precise, and accurate identification of specific behaviors. Machine learning-based platforms like DeepLabCut and SimBA make it possible to extract frame-by frame behavior data from recorded videos, allowing for discrete neural events to be mapped onto corresponding behavior with high temporal precision. An advantage of using these platforms is that models can be easily developed to identify any behavior of interest, thus they are highly flexible and can be used for a variety of applications. Here, we develop an analysis pipeline that allows us to compare freezing to photometry data in two different ways; by aligning spiking, and by calculating average activity during different behavioral states. Using the spike alignment method, we show that vPAG^{VGAT} spike frequency is lower during freezing compared to mobility. Complementary to this, we find the same effect in vPAG terminals in the CeA using the averaging method. These techniques provide a framework for parsing fiber photometry recordings that can accommodate different types of in vivo imaging data.

The present study does not examine sex differences, and thus is limited in scope. As many preclinical fear studies have focused solely on males, significantly less is known about the circuitry underlying fear learning in females. It has been previously shown that female rats show increased darting behavior during fear learning than males [50], thus we might expect more

activity in the vPAGVGAT-CeA pathway in females. Additionally, clinical studies have reported higher 5HT levels, higher serotonin transporter availability, and greater efficacy of selective serotonin reuptake inhibitors in women than men [51], highlighting sex differences in 5HT signaling. As such, we might expect to see differences in 5HT release during fear learning in females, and differential modulation of the vPAGVGAT-CeA pathway by 5HT.

In conclusion, our study characterizes a novel GABAergic input to the CeA from the vPAG that is engaged during fear learning and is modulated by presynaptic $5HT_{2C}$. These findings provide initial evidence that the vPAG has modulatory influence over fear learning through inputs to the CeA. As such, the vPAG is not a mere effector that executes commands from the CeA to drive fear expression but rather may shape the learning processes by encoding responses to aversive stimuli. Given the reciprocal interactions between the vPAG and CeA and their established roles in fear learning and expression, dysregulation of the $vPAG^{VGAT}$-CeA input may contribute to the pathophysiology of post-traumatic stress and other fear-related disorders and therefore may be a novel target for therapeutic interventions.

REFERENCES

1. Herry C, Johansen JP. Encoding of fear learning and memory in distributed neuronal circuits. Nat Neurosci. 2014;17:1644–54.
2. Martinez RC, de Oliveira AR, Brandao ML. Conditioned and unconditioned fear organized in the periaqueductal gray are differentially sensitive to injections of muscimol into amygdaloid nuclei. Neurobiol Learn Mem. 2006; 85:58–65.
3. Dejean C, Courtin J, Rozeske RR, Bonnet MC, Dousset V, Michelet T, et al. Neuronal Circuits for Fear Expression and Recovery: Recent Advances and Potential Therapeutic Strategies. Biol Psychiatry. 2015;78:298–306.
4. Tovote P, Fadok JP, Luthi A. Neuronal circuits for fear and anxiety. Nat Rev Neurosci. 2015;16:317–31.
5. George DT, Ameli R, Koob GF. Periaqueductal Gray Sheds Light on Dark Areas of Psychopathology. Trends Neurosci. 2019;42:349–60.
6. LeDoux JE, Iwata J, Cicchetti P, Reis DJ. Different projections of the central amygdaloid nucleus mediate autonomic and behavioral correlates of conditioned fear. J Neurosci. 1988;8:2517–29.
7. Vianna DM, Graeff FG, Landeira-Fernandez J, Brandao ML. Lesion of the ventral periaqueductal gray reduces conditioned fear but does not change freezing induced by stimulation of the dorsal periaqueductal gray. Learn Mem. 2001;8:164–9.
8. Zanoveli JM, Carvalho MC, Cunha JM, Brandao ML. Extracellular serotonin level in the basolateral nucleus of the amygdala and dorsal periaqueductal gray under unconditioned and conditioned fear states: an in vivo microdialysis study. Brain Res. 2009;1294:106–15.
9. Ciocchi S, Herry C, Grenier F, Wolff SB, Letzkus JJ, Vlachos I, et al. Encoding of conditioned fear in central amygdala inhibitory circuits. Nature. 2010;468:277–82.
10. Kim EJ, Horovitz O, Pellman BA, Tan LM, Li Q, Richter-Levin G, et al. Dorsal periaqueductal gray-amygdala pathway conveys both innate and learned fear responses in rats. Proc Natl Acad. 2013;110:14795–14800.
11. Haubensak W, Kunwar PS, Cai H, Ciocchi S, Wall NR, Ponnusamy R, et al. Genetic dissection of an amygdala microcircuit that gates conditioned fear. Nature. 2010;468:270–6.
12. Li H, Penzo MA, Taniguchi H, Kopec CD, Huang ZJ, Li B. Experience-dependent modification of a central amygdala fear circuit. Nat Neurosci. 2013;16:332–9.
13. Penzo MA, Robert V, Li B. Fear conditioning potentiates synaptic transmission onto long-range projection neurons in the lateral subdivision of central amygdala. J Neurosci. 2014;34:2432–7.
14. Penzo MA, Robert V, Tucciarone J, De Bundel D, Wang M, Van Aelst L, et al. The paraventricular thalamus controls a central amygdala fear circuit. Nature. 2015;519:455–9.
15. Johansen JP, Tarpley JW, LeDoux JE, Blair HT. Neural substrates for expectation-modulated fear learning in the amygdala and periaqueductal gray. Nat Neurosci. 2010;13:979–86.
16. McNally GP, Johansen JP, Blair HT. Placing prediction into the fear circuit. Trends Neurosci. 2011;34:283–92.
17. Roy M, Shohamy D, Daw N, Jepma M, Wimmer GE, Wager TD. Representation of aversive prediction errors in the human periaqueductal gray. Nat Neurosci. 2014;17:1607–12.
18. Rizvi TA, Ennis M, Behbehani MM, Shipley MT. Connections between the central nucleus of the amygdala and the midbrain periaqueductal gray: topography and reciprocity. J Comp Neurol. 1991;303:121–31.
19. Bienkowski MS, Rinaman L. Common and distinct neural inputs to the medial central nucleus of the amygdala and anterior ventrolateral bed nucleus of stria terminalis in rats. Brain Struct Funct. 2013;218:187–208.
20. Fu W, Le Maitre E, Fabre V, Bernard JF, David Xu ZQ, Hokfelt T. Chemical neuroanatomy of the dorsal raphe nucleus and adjacent structures of the mouse brain. J Comp Neurol. 2010;518:3464–94.
21. Challis C, Boulden J, Veerakumar A, Espallergues J, Vassoler FM, Pierce RC, et al. Raphe GABAergic neurons mediate the acquisition of avoidance after social defeat. J Neurosci. 2013;33:13978–88, 13988a.
22. Lowery-Gionta EG, DiBerto J, Mazzone CM, Kash TL. GABA neurons of the ventral periaqueductal gray area modulate behaviors associated with anxiety and conditioned fear. Brain Struct Funct. 2018;223:3787–99.
23. Tovote P, Esposito MS, Botta P, Chaudun F, Fadok JP, Markovic M, et al. Midbrain circuits for defensive behaviour. Nature. 2016;534:206–12.
24. Burghardt NS, Bauer EP. Acute and chronic effects of selective serotonin reuptake inhibitor treatment on fear conditioning: implications for underlying fear circuits. Neuroscience. 2013;247:253–72.
25. Marcinkiewcz CA, Mazzone CM, D'Agostino G, Halladay LR, Hardaway JA, DiBerto JF, et al. Serotonin engages an anxiety and fear-promoting circuit in the extended amygdala. Nature. 2016;537:97–101.
26. Marcinkiewcz CA, Bierlein-De La Rosa G, Dorrier CE, McKnight M, DiBerto JF, Pati D, et al. Sex-Dependent Modulation of Anxiety and Fear by 5-HT1A Receptors in the Bed Nucleus of the Stria Terminalis. ACS Chem Neurosci. 2019;10:3154–66.
27. Unger EK, Keller JP, Altermatt M, Liang R, Matsui A, Dong C, et al. Directed Evolution of a Selective and Sensitive Serotonin Sensor via Machine Learning. Cell. 2020;183:1986–2002.e26.
28. Ren J, Friedmann D, Xiong J, Liu CD, Ferguson BR, Weerakkody T, et al. Anatomically Defined and Functionally Distinct Dorsal Raphe Serotonin Sub-systems. Cell. 2018;175:472–87 e20.
29. Rainnie DG. Serotonergic modulation of neurotransmission in the rat basolateral amygdala. J Neurophysiol. 1999;82:69–85.
30. Spoida K, Masseck OA, Deneris ES, Herlitze S. Gq/5-HT2c receptor signals activate a local GABAergic inhibitory feedback circuit to modulate serotonergic firing and anxiety in mice. Proc Natl Acad Sci. 2014;111:6479–84.
31. Theile JW, Morikawa H, Gonzales RA, Morrisett RA. Role of 5-hydroxytryptamine2C receptors in Ca2+-dependent ethanol potentiation of GABA release onto ventral tegmental area dopamine neurons. J Pharm Exp Ther. 2009;329:625–33.
32. Vong L, Ye C, Yang Z, Choi B, Chua S, Lowell BB. Leptin action on GABAergic neurons prevents obesity and reduces inhibitory tone to POMC neurons. Neuron. 2011;71:142–54.
33. Mathis A, Mamidanna P, Cury KM, Abe T, Murthy VN, Mathis MW, et al. DeepLabCut: markerless pose estimation of user-defined body parts with deep learning. Nat Neurosci. 2018;21:1281–9.
34. Nilsson SR, Goodwin NL, Choong JJ, Hwang S, Wright HR, Norville ZC, et al. Simple Behavioral Analysis (SimBA) – an open source toolkit for computer classification of complex social behaviors in experimental animals. 2020. bioRxiv. https://doi.org/10.1101/2020.04.19.049452.
35. Martianova E, Aronson S, Proulx CD Multi-Fiber Photometry to Record Neural Activity in Freely-Moving Animals. J Vis Exp JoVE. 2019. 20 October 2019. https://doi.org/10.3791/60278.
36. Lowery-Gionta EG, Marcinkiewcz CA, Kash TL. Functional alterations in the dorsal raphe nucleus following acute and chronic ethanol exposure. Neuropsychopharmacology. 2015;40:590–600.
37. Lowery-Gionta EG, Crowley NA, Bukalo O, Silverstein S, Holmes A, Kash TL. Chronic stress dysregulates amygdalar output to the prefrontal cortex. Neuropharmacology. 2018;139:68–75.
38. Khom S, Wolfe SA, Patel RR, Kirson D, Hedges DM, Varodayan FP, et al. Alcohol Dependence and Withdrawal Impair Serotonergic Regulation of GABA Transmission in the Rat Central Nucleus of the Amygdala. J Neurosci. 2020;40:6842–53.
39. Barnes NM, Sharp T. A review of central 5-HT receptors and their function. Neuropharmacology. 1999;38:1083–152.
40. Nicholson AA, Friston KJ, Zeidman P, Harricharan S, McKinnon MC, Densmore M, et al. Dynamic causal modeling in PTSD and its dissociative subtype: Bottom-up versus top-down processing within fear and emotion regulation circuitry. Hum Brain Mapp. 2017;38:5551–61.
41. Sengupta A, Holmes A. A Discrete Dorsal Raphe to Basal Amygdala 5-HT Circuit Calibrates Aversive Memory. Neuron. 2019;103:489–505.e7.

42. Amat J, Matus-Amat P, Watkins LR, Maier SF. Escapable and inescapable stress differentially alter extracellular levels of 5-HT in the basolateral amygdala of the rat. Brain Res. 1998;812:113–20.
43. Tokunaga R, Shimoju R, Takagi N, Shibata H, Kurosawa M. Serotonin release in the central nucleus of the amygdala in response to noxious and innocuous cutaneous stimulation in anesthetized rats. J Physiol Sci. 2016;66:307–14.
44. Ren J, Isakova A, Friedmann D, Zeng J, Grutzner SM, Pun A, et al. Single-cell transcriptomes and whole-brain projections of serotonin neurons in the mouse dorsal and median raphe nuclei. ELife. 2019;8:e49424.
45. Becamel C, Gavarini S, Chanrion B, Alonso G, Galeotti N, Dumuis A, et al. The serotonin 5-HT2A and 5-HT2C receptors interact with specific sets of PDZ proteins. J Biol Chem. 2004;279:20257–66.
46. Namburi P, Beyeler A, Yorozu S, Calhoon GG, Halbert SA, Wichmann R, et al. A circuit mechanism for differentiating positive and negative associations. Nature. 2015;520:675–8.
47. Duvarci S, Popa D, Pare D. Central amygdala activity during fear conditioning. J Neurosci. 2011;31:289–94.
48. Wright KM, McDannald MA. Ventrolateral periaqueductal gray neurons prioritize threat probability over fear output. ELife. 2019;8:e45013.
49. Wright KM, Jhou TC, Pimpinelli D, McDannald MA. Cue-inhibited ventrolateral periaqueductal gray neurons signal fear output and threat probability in male rats. ELife. 2019;8:e50054.
50. Gruene TM, Flick K, Stefano A, Shea SD, Shansky RM. Sexually divergent expression of active and passive conditioned fear responses in rats. ELife. 2015;4:e11352.
51. Sramek JJ, Murphy MF, Cutler NR. Sex differences in the psychopharmacological treatment of depression. Dialogues Clin Neurosci. 2016;18:447–57.

ACKNOWLEDGEMENTS

Schematics for this manuscript were created using Biorender.com.

AUTHOR CONTRIBUTIONS

OJH, EGLG and TLK: designed the experiments. OJH, EGLG, JFD, JS, DWB, MH, AK, NMM and AJL: performed the experiments. OJH, EGLG, JFD, CMM and JAH: analyzed data. OJH, EGLG and TLK: interpreted the data and wrote the manuscript.

FUNDING

This work was supported by the Bowles Center for Alcohol Studies and NIAAA/ NIH: F32-AA022549 (EGLG); T32-AA007573 (EGLG); R01-AA019454 (TLK); U01-AA020911 (TLK); P60-AA011605 (TLK); T32-NS007431 (OJH).

COMPETING INTERESTS

The authors declare no competing interests.

ADDITIONAL INFORMATION

Supplementary information The online version contains supplementary material available at https://doi.org/10.1038/s41386-022-01392-4.

Correspondence and requests for materials should be addressed to Emily G. Lowery-Gionta.

Reprints and permission information is available at http://www.nature.com/reprints

Publisher's note Springer Nature remains neutral with regard to jurisdictional claims in published maps and institutional affiliations.